MNRAS **000**, 000–000 (2024) Preprint 18 May 2023 Compiled using MNRAS LATEX style file v3.0

The CO-to-H_2 Conversion Factor of the Galactic Giant Molecular Clouds using CO isotopologues: the high-resolution X_{CO} maps

Mikito Kohno[1,2]★, and Yoshiaki Sofue[3]
[1]*Astronomy Section, Nagoya City Science Museum, 2-17-1 Sakae, Naka-ku, Nagoya, Aichi 460-0008, Japan*
[2]*Department of Physics, Graduate School of Science, Nagoya University, Furo-cho, Chikusa-ku, Nagoya, Aichi 464-8602, Japan*
[3]*Institute of Astronomy, The University of Tokyo, Mitaka, Tokyo 181-0015, Japan*

Accepted 2023. Received 2023; in original form 2023

ABSTRACT
We investigated the correlation between intensities of the ^{12}CO and ^{13}CO (J = 1-0) lines toward the Galactic giant molecular clouds (GMCs) W51A, W33, N35-N36 complex, W49, M17SW, G12.02-00.03, W43, and M16 using the FUGIN (FOREST Unbiased Galactic plane Imaging survey with the Nobeyama 45-m telescope) CO line data. All the GMCs showed intensity saturation in the ^{12}CO line when the brightness temperature of ^{13}CO is higher than a threshold temperature of about $\sim$ 5 K. We obtained high-resolution ($\sim$ 20″) distribution maps of the X_{CO} factor in individual GMCs using the correlation diagrams of the CO isotopologues. It was shown that X_{CO} is variable in each GMC within the range of $X_{CO} \sim (0.9–5) \times 10^{20}$ cm^{-2} (K km s^{-1})$^{-1}$. Despite the variability in the GMCs, the averaged value among the GMCs was found to be nearly constant at $X_{CO} = (2.16 \pm 0.30) \times 10^{20}$ cm^{-2} (K km s^{-1})$^{-1}$, which is consistent with that from the previous studies in the Milky Way.

Key words: ISM: clouds – ISM: general – ISM: molecules – radio lines: ISM

1 INTRODUCTION

Molecular clouds mainly consist of hydrogen molecules (H_2) and are the sites of star formation in galaxies (Blitz et al. 2007; Dobbs et al. 2014; Chevance et al. 2022). The hydrogen molecule is difficult to observe directly because it does not have an electric dipole moment for its homonuclear diatomic nature (Heyer & Dame 2015). Therefore, we often observe carbon monoxide (CO) with the rotational transitions at millimeter wavelengths and convert the intensity to the H_2 column density using the CO-to-H_2 conversion factor (hereafter X_{CO}), which is given by

$$X_{CO} = N_{H_2}/W_{^{12}CO} \ [\mathrm{cm^{-2}\ (K\ km\ s^{-1})^{-1}}], \quad (1)$$

where $W_{^{12}CO}$ and N_{H_2} are the ^{12}CO J =1-0 integrated intensity and column density of hydrogen molecule, respectively (Bolatto et al. 2013).

The conversion factor has been obtained in various ways by comparisons of CO luminosity with virial mass (e.g.,Solomon et al. 1987; Scoville et al. 1987), visual or infrared extinction (e.g.,Frerking et al. 1982; Lombardi et al. 2006; Pineda et al. 2008; Lee et al. 2018), X-ray absorption (e.g.,Sofue & Kataoka 2016), the brightness of gamma-ray (e.g.,Strong et al. 1988; Abdo et al. 2010; Planck Collaboration et al. 2015; Hayashi et al. 2019), and dust emission (e.g.,Planck Collaboration et al. 2011; Fukui et al. 2014; Okamoto et al. 2017; Hayashi et al. 2019). The values have been discussed in the Milky Way and Local Group galaxies, and the dependence on the metallicity has been suggested (e.g.,Wilson 1995; Arimoto et al. 1996; Sakamoto 1996; Dame et al. 2001; Mizuno et al. 2001; Rosolowsky et al. 2003; Fukui & Kawamura 2010; Liszt et al. 2010; Leroy et al. 2011; Lee et al. 2014; Lin et al. 2016; Muraoka et al. 2017; Pitts & Barnes 2021; Ohno et al. 2023). The often used value currently in the Milky Way is $X_{CO} = 2.0\times10^{20}$ cm^{-2} (K km s^{-1})$^{-1}$, having uncertainty of ±30% (Bolatto et al. 2013).

Recently, Sofue & Kohno (2020)(hereafter paper I) proposed a new method to estimate the molecular cloud mass considering the variability of the X_{CO} factor from the correlation between ^{12}CO and ^{13}CO. Paper I analyzed only two Galactic GMCs of M16 (Sofue 2020b; Nishimura et al. 2021) and W43(Sofue et al. 2019; Sofue 2021; Kohno et al. 2021), and the spatial distributions of X_{CO} inside the GMCs have not been discussed yet.

In this paper, we extend the analysis of Paper I, aiming at revealing the variability of X_{CO} within the molecular cloud of scales ($\sim$ 10-50 pc) at sub-pc resolutions ($\sim$ 20″). The target GMCs are W51A (Fujita et al. 2021), W33 (Kohno et al. 2018), W49 (Miyawaki et al. 2022), N35-N36 complex (Torii et al. 2018; Sofue 2019a,b), M17SW (Nishimura et al. 2018; Sofue 2020a, 2022), G012.02-00.03(Sanna et al. 2014), W43(Sofue et al. 2019; Kohno et al. 2021), and M16(Sofue 2020b; Nishimura et al. 2021). These GMCs are also known as the massive star-forming regions in the Milky Way. The basic parameters of these GMCs were summarized in Table 1.

This paper is structured as follows: section 2 introduces the FUGIN (FOREST Unbiased Galactic plane Imaging survey with

★ E-mail: mikito.kohno@gmail.com, kohno@nagoya-p.jp

© 2024 The Authors

the Nobeyama 45-m telescope) data; section 3 presents the methods of analysis; in section 4, we demonstrate the results; in section 5, we discuss the variability of the $X_{\rm CO}$ factor, and in section 6, we summarize the results.

2 DATA

We utilized the ^{12}CO, ^{13}CO J =1-0 line data obtained with the Nobeyama 45 m telescope (FUGIN: Umemoto et al. 2017; Torii et al. 2019; Fujita et al. 2023). The front end was the FOur beam REceiver System on the 45-m Telescope (FOREST: Minamidani et al. 2016; Nakajima et al. 2019), which is the four-beam, side-band separating (2SB), and dual-polarization superconductor–insulator–superconductor (SIS) receiver. The observations were carried out in the on-the-fly mapping mode (Sawada et al. 2008). The back-end system used an FX-type spectrometer named SAM 45 (Kuno et al. 2011; Kamazaki et al. 2012). The data were calibrated to the main-beam temperature by measuring the main-beam efficiency of 0.43 for ^{12}CO, 0.45 for ^{13}CO, and C^{18}O using the standard calibration sources. The detailed information on the FUGIN project was summarized in the project overview paper by Umemoto et al. (2017). The cube data calibrated to the main-beam temperature is opened at the Japanese Virtual Observatory (JVO). The root-mean-square noise level of each GMC was presented in Table 1.

3 METHODS

We derive the H_2 column density per velocity channel by the local thermal equilibrium (LTE) method using the $X_{\rm CO}$ factor as based in Paper I and Pineda et al. (2008). The brightness temperature ($T_{\rm B}$) of CO line intensity with the excitation temperature ($T_{\rm ex}$) and optical depth (τ) is given by

$$T_{\rm B} = T_0 \left(\frac{1}{e^{T_0/T_{\rm ex}} - 1} - \frac{1}{e^{T_0/T_{\rm bg}} - 1} \right) (1 - e^{-\tau}) \ [{\rm K}], \quad (2)$$

where $T_{\rm bg}$ = 2.725 K is the temperature of the cosmic-microwave background radiation. $T_0 = h\nu/k$ is the Planck temperature with h, ν, and k being the Planck constant, rest frequency, and Boltzman constant, respectively. If we assume the ^{12}CO line is optically thick, the excitation temperature is given by

$$T_{\rm ex} = T_0^{115} \Big/ \ln \left(1 + \frac{T_0^{115}}{T_{\rm B}(^{12}{\rm CO})_{\rm max} + 0.83632} \right) \ [{\rm K}], \quad (3)$$

where $T_{\rm B}(^{12}{\rm CO})_{\rm max}$ and T_0^{115} = 5.53194 correspond to the ^{12}CO peak intensity and the Planck temperature at the rest frequency of ^{12}CO J =1-0, respectively. We assume that $T_{\rm ex}$ is equal in the ^{12}CO and ^{13}CO line emissions, and express the optical depth as

$$\tau(^{13}{\rm CO}) = -\ln \left(1 - \frac{T_{\rm B}(^{13}{\rm CO})_{\rm max}/T_0^{110}}{(e^{T_0^{110}/T_{\rm ex}} - 1)^{-1} - 0.167667} \right), \quad (4)$$

where $T_{\rm B}(^{13}{\rm CO})_{\rm max}$ and T_0^{110} = 5.28864 represent the ^{13}CO peak intensity and the Planck temperature at the rest frequency of ^{13}CO J =1-0, respectively. The ^{13}CO column density is given by

$$N_{^{13}{\rm CO}} = 3.0 \times 10^{14} \ \frac{\tau}{1 - e^{-\tau}} \frac{1}{1 - e^{-T_0^{110}/T_{\rm ex}}} \ I_{^{13}{\rm CO}} \ [{\rm cm}^{-2}], \quad (5)$$

where $I_{^{13}{\rm CO}}$ is the ^{13}CO integrated intensity. Then, we convert $N_{^{13}{\rm CO}}$ to the H_2 column density using the abundance ratio of H_2 to ^{13}CO molecules given by

$$N_{\rm H_2}(^{13}{\rm CO}) = Y_{^{13}{\rm CO}} N_{^{13}{\rm CO}} \ [{\rm cm}^{-2}]. \quad (6)$$

Here, $Y_{^{13}{\rm CO}}$ is adopted as (5.0±2.5)×10^5 (Dickman 1978) following Paper I.

We, then, calculate the H_2 column density per velocity channel, which is defined as the spectral column density, using the LTE method for $X_{\rm CO}$ from the intensity of ^{12}CO and ^{13}CO as in Paper I. The spectral column densities (SCD) of ^{12}CO and ^{13}CO are expressed as

$${\rm SCD_{12X}} = \frac{dN_{\rm H_2}(^{12}{\rm CO})}{dv} = X_{\rm CO} T_{\rm B}(^{12}{\rm CO}) \ [{\rm cm}^{-2}({\rm km\ s}^{-1})^{-1}], \quad (7)$$

and

$${\rm SCD_{13L}} = \frac{dN_{\rm H_2}(^{13}{\rm CO})}{dv} = 3.0 \times 10^{14} \ \frac{\tau}{1 - e^{-\tau}} \frac{Y_{^{13}{\rm CO}} T_{\rm B}(^{13}{\rm CO})}{1 - e^{-T_0^{110}/T_{\rm ex}}} \ [{\rm cm}^{-2}({\rm km\ s}^{-1})^{-1}]. \quad (8)$$

Here, SCD$_{\rm 12X}$ and SCD$_{\rm 13L}$ are spectral column densities of H_2 at the peak velocity channels, derived from the $X_{\rm CO}$ factor and the LTE assumption, respectively.

4 RESULTS

Figure 1(a-h) shows thus obtained ^{12}CO J =1-0 peak intensity maps of W51A, W33, N35-N36 complex, W49, M17SW, G012.02-00.03, W43 and M16 GMC. W49 and G012.02-00.03 GMC show compact CO distribution of ∼ 20 pc, while W33, N35-N36 complex, W43, and M16 have more diffuse distribution of molecular gas at 15-20 K, 10-15 K, 15-18 K, and 10-20 K of the brightness temperature, respectively.

Figure 2(a-h) presents scatter plots between SCD$_{\rm 12X}$ and SCD$_{\rm 13L}$ of GMCs presented in Figure1(a-h). Black dotted lines show the linear relation of SCD$_{\rm 12X}$ = SCD$_{\rm 13L}$. SCD$_{\rm 12X}$ shows saturation at high SCD$_{\rm 13L}$, and the nonlinear relation of each GMC has different saturation levels. The nonlinear relation between the ^{12}CO and ^{13}CO intensity are consistent with the previous studies on the Perseus molecular clouds (Pineda et al. 2008) and the CO J =2-1 Galactic plane survey (Yoda et al. 2010). Then, we performed curve fitting to the scatter plots between SCD$_{\rm 12X}$ and SCD$_{\rm 13L}$ using the free parameters of α and SCD$_{\rm c}$(spectral column density coefficient), as in Paper I. SCD$_{\rm 12X}$ is given by

$${\rm SCD_{12X}} = {\rm SCD_c} \left(\frac{\rm SCD_{13L}}{\rm SCD_c} \right)^{\alpha}. \quad (9)$$

The blue curves show the fitting results of individual GMCs. The fitting parameters have the range of α = 0.29-0.60 and SCD$_{\rm c}$=(1.2-4.8) × 10^{21}cm^{-2} (km s^{-1})$^{-1}$.

5 DISCUSSION

5.1 Spatial distributions of $X_{\rm CO}$ in the Galactic GMCs

We obtained the $X_{\rm CO}$ factor of each GMC from the correlation between SCD$_{\rm 12X}$ and SCD$_{\rm 13L}$. The $X_{\rm CO}$ factor at each pixel of

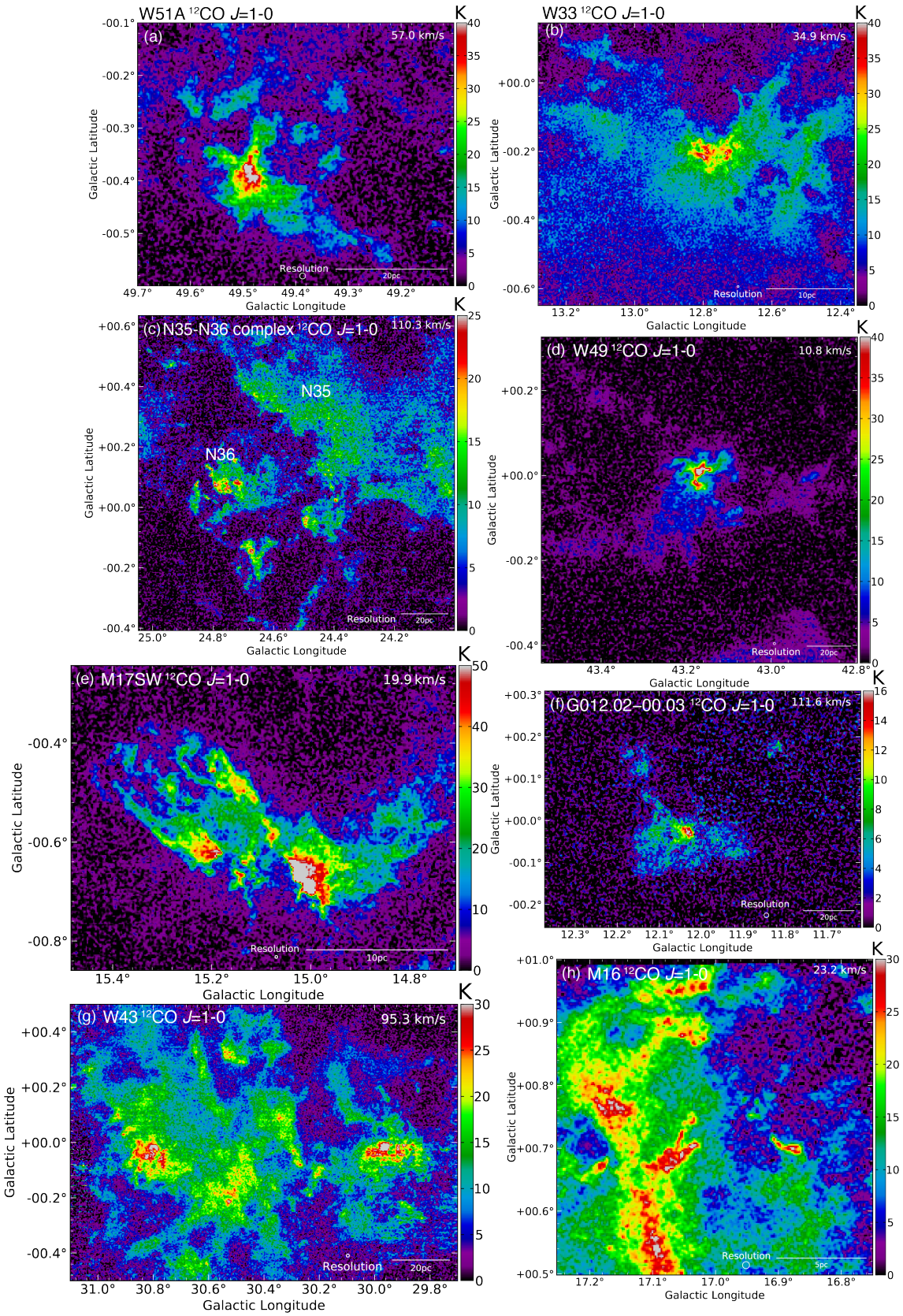

Figure 1. The ^{12}CO peak intensity map of (a) W51A at the radial velocity of 57.0 km s^{-1}, (b) W33 at 34.9 km s^{-1}, (c) N35-N36 complex at 110.3 km s^{-1}, (d) W49 at 10.8 km s^{-1}, (e) M17SW at 19.9 km s^{-1}, (f) G012.02-00.03 at 111.6 km s^{-1},(g) W43 at 95.3 km s^{-1}, and (h) M16 at 23.2 km s^{-1}.

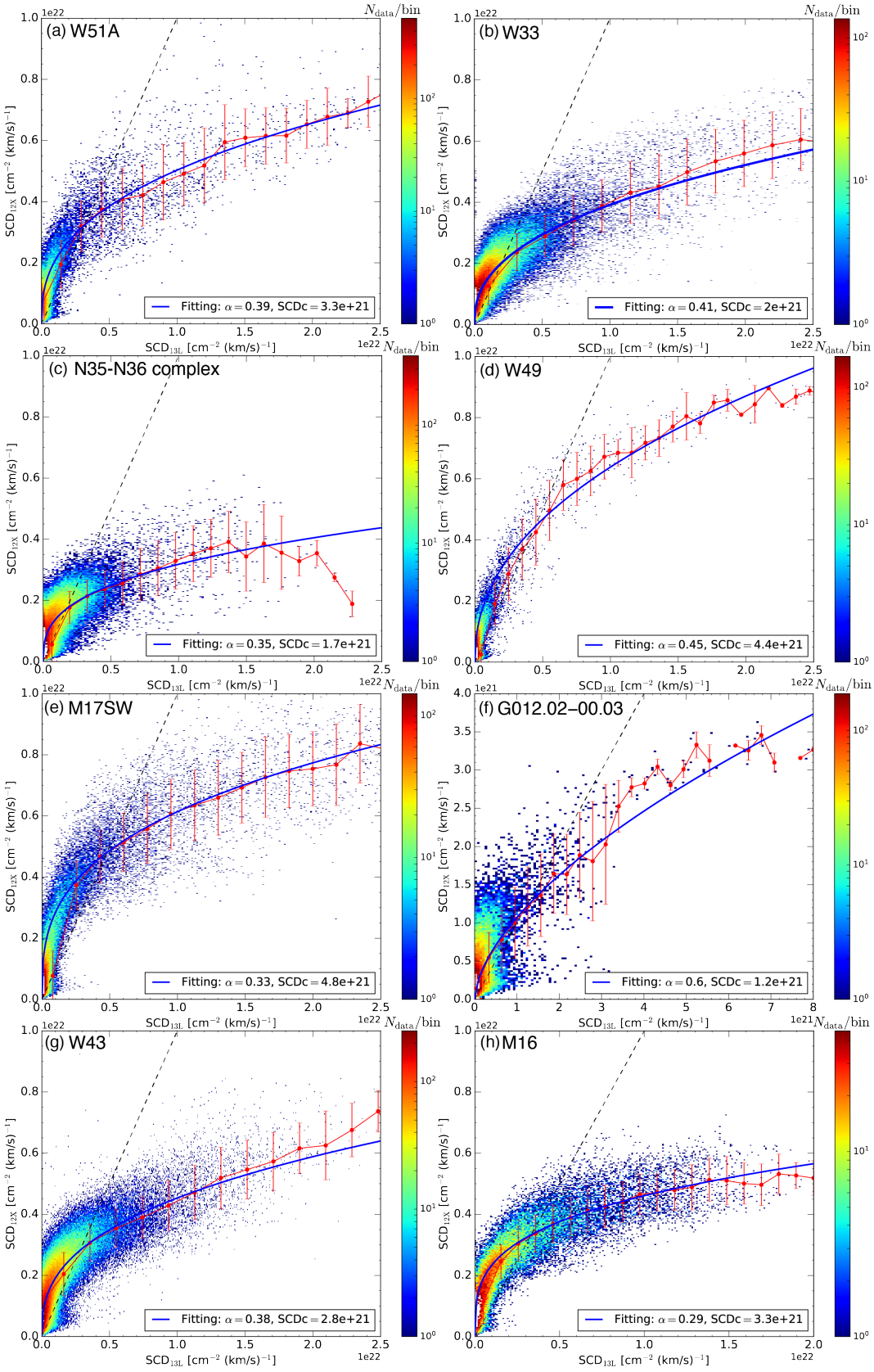

Figure 2. Scatter plot between SCD_{13L} and SCD_{12X} of (a) W51A, (b) W33, (c) the N35-N36 complex, (d) W49, (e) M17SW, (f) G012.02-00.03, (g) W43, and (h) M16. Red points show the averaged values of each bin, and the error bars are standard deviations of SCD_{12X}. Blue curves indicate the fitting results of scatter plots. The black dashed lines indicate the lenear relation of SCD_{12X} =SCD_{13L}.

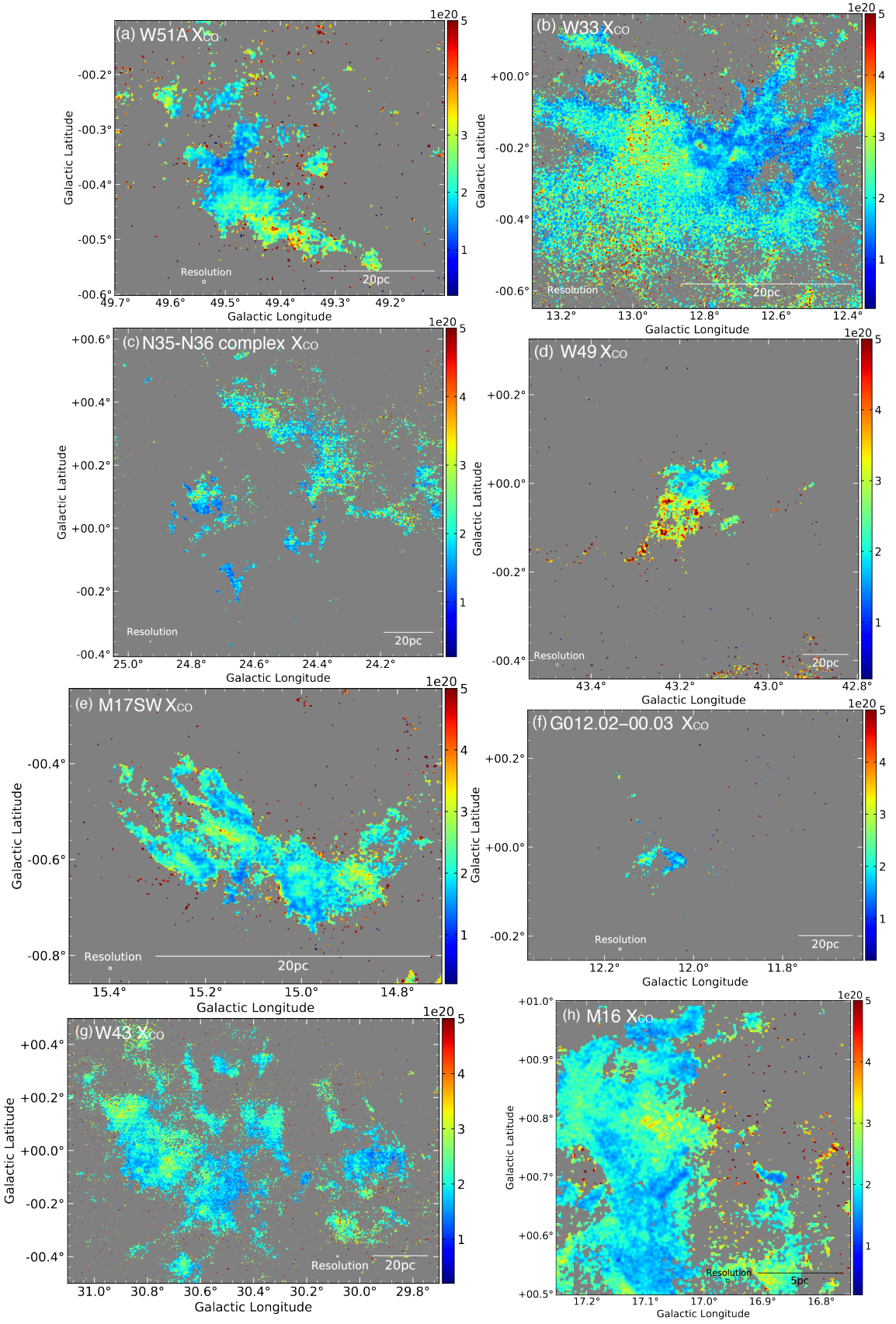

Figure 3. Spatial distributions of the X_{CO} factor in (a) W51A, (b) W33, (c) the N35-N36 complex, (d) W49, (e) M17SW, (f) G012,02-00.03, (g) W43, and (h) M16. The points are plotted of T_B (^{13}CO) $> 3\sigma$. The 1σ noise level of each GMC is presented in Table 1.

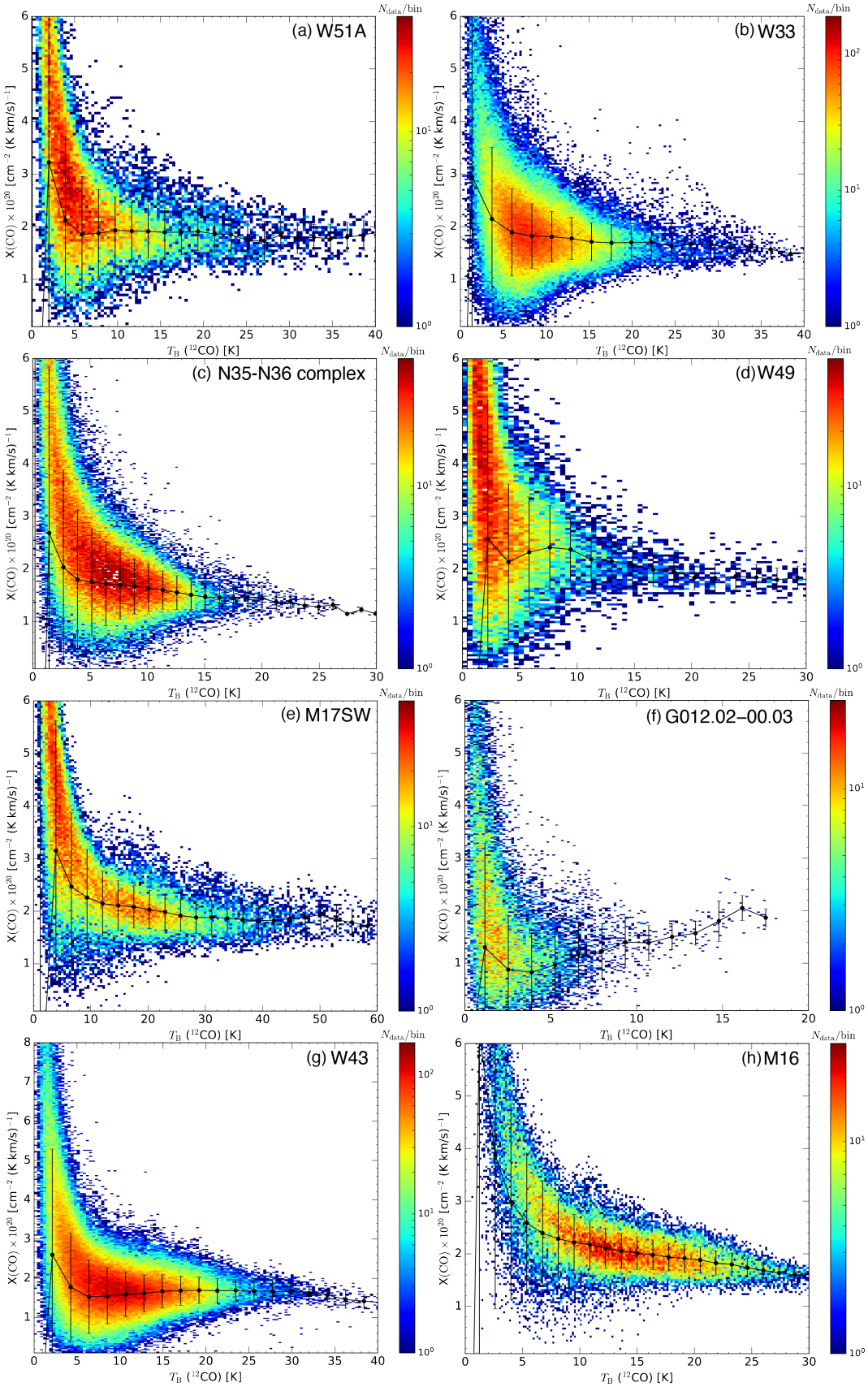

Figure 4. Scatter plot between the $X_{\rm CO}$ factor and $T_{\rm B}$ (^{12}CO) in (a) W51A, (b) W33, (c) the N35-N36 complex, (d) W49, (e) M17SW, (f) G012,02-00.03, (g) W43, and (h) M16. Black points show the averaged values of each bin, and the error bars are standard deviations of the $X_{\rm CO}$ factor.

Table 1. Properties of the Galactic massive star forming regions

Name	l	b	$V_{\rm LSR}$	D	$R_{\rm G}$	$T_{\rm rms}$ (^{13}CO)	Reference
	[deg]	[deg]	[km s^{-1}]	[kpc]	[kpc]	[K]	
(1)	(2)	(3)	(4)	(5)	(6)	(7)	(8)
W51A	49.5	−0.4	57	5.4	6.1	~ 0.6	[1]
W33	12.8	−0.2	35	2.4	5.7	~ 0.6	[2]
N35-N36 complex	24.5	0.1	110	7.3	3.3	~ 1.1	[3,4]
W49A	43.16	0.0	11	11	7.5	~ 0.5	[5]
M17SW	15.0	−0.7	20	2.0	6.1	~ 0.7	[6,7,8]
G012.02−00.03	12.02	`0.03	112	9.4	2.3	~ 0.7	[9]
W43	30.8	0.0	95	5.5	4.3	~ 0.9	[10,11]
M16	17.1	0.7	23	2.0	6.1	~ 0.7	[12,13]

Columns: (1) Name. (2) Galactic longitude (3) Galactic latitude (4) Radial velocity (5) Distance from the solar system (6) Distance from the Galactic center. The Galactric distance from the Sun is assumed to be R_0 = 8.0 kpc obtained by the mean value of the very long baseline interferometry astrometry results (VERA Collaboration et al. 2020; Reid et al. 2019). (7) r.m.s noise reveals of the ^{13}CO data (8) References [1] Fujita et al. (2021) [2] Kohno et al. (2018) [3] Torii et al. (2018) [4] Sofue (2019a) [5] Miyawaki et al. (2022) [6] Nishimura et al. (2018) [7] Sofue (2020a) [8] Yamagishi et al. (2016) [9] Sanna et al. (2014) [10] Sofue et al. (2019) [11]Kohno et al. (2021) [12] Sofue (2020b)[13] Nishimura et al. (2021)

molecular clouds is expressed as

$$X_{\rm CO} = {\rm SCD_c}\left(\frac{\rm SCD_{13L}}{\rm SCD_c}\right)^{\alpha} \Big/ T_{\rm B}(^{12}{\rm CO})\ [{\rm cm^{-2}(K\ km\ s^{-1})^{-1}}]. \quad (10)$$

where α and SCD$_c$ are the fitting parameters obtained in Figure 2.

Figure 3(a-h) shows the $X_{\rm CO}$ maps of each GMC. $X_{\rm CO}$ has a variability with the range of (0.9-5.0) $\times 10^{20}$ [cm^{-2}(K km s^{-1})$^{-1}$] in a GMC. Comparing Figure 1 and Figure 3, we find an anti-correlation between the ^{12}CO peak intensity and $X_{\rm CO}$. Figure 4 shows the scatter plot between the $X_{\rm CO}$ factor and T_B (^{12}CO) in each GMC. The $X_{\rm CO}$ factor monotonically decreases with increasing brightness temperature except for G012.02-00.03. It also shows a lower limit around $X_{\rm CO} \sim 2 \times 10^{20}$cm^{-2} (K km s^{-1})$^{-1}$ above $T(^{12}{\rm CO}) > 20$ K. These results may correspond to the saturation of ^{12}CO intensity in dense cores of the GMC. It is consistent with previous studies of the Perseus molecular clouds obtained by the correlation between the ^{12}CO integrated intensity and H$_{\rm I}$ column number density derived from the optical depth of 353 GHz dust emission (τ_{353}) by the Planck satellite observations (see Figure 12 and 15 in Okamoto et al. 2017).

Table 2 lists the results of parameter fitting for α, SCD$_{\rm c}$, $X_{\rm CO}$, and correlation coefficient. The mean value of $X_{\rm CO}$ of all GMCs in this paper is $(2.16 \pm 0.30) \times 10^{20}$ cm^{-2} (K km s^{-1})$^{-1}$. In our study, $X_{\rm CO}$ shows the local variability in the Galactic GMCs (Figure3), while the mean value is consistent within errors previous works reported 2×10^{20} cm^{-2} (K km s^{-1})$^{-1}$ (Bolatto et al. 2013), $(1.8 \pm 0.3) \times 10^{20}$ cm^{-2} (K km s^{-1})$^{-1}$ (Dame et al. 2001), and $(2.54 \pm 0.13) \times 10^{20}$ cm^{-2} (K km s^{-1})$^{-1}$ (Planck Collaboration et al. 2011).

5.2 Radial gradient of the $X_{\rm CO}$ factor

Finally, we investigated the radial gradient of the $X_{\rm CO}$ factor in the Galactic disc. The averaged $X_{\rm CO}$ factor has a high value in W49 at Galactocentric distance R =7.5 kpc, while G012.02-00.03 has a low value a R =2.3 kpc. According to Arimoto et al. (1996), the $X_{\rm CO}$ factor increases with the Galactocentric radius by an exponential function given by

$$\log_{10}\left(\frac{X_{\rm CO}}{X_0}\right) = 0.41\frac{(R-R_0)}{r_e}, \quad (11)$$

Table 2. Fitting results and <$X_{\rm CO}$> taken from the correlation of SCD$_{\rm 12X}$ and SCD$_{\rm 13L}$.

Name	α	SCD$_{\rm C}$ [$\times 10^{21}$]	$< X({\rm CO}) >$ [$\times 10^{20}$]	C.C
(1)	(2)	(3)	(4)	(5)
W51A	0.39	3.3	2.23	0.76
W33	0.41	2.0	2.14	0.74
N35-N36	0.35	1.7	2.13	0.71
W49	0.45	4.4	2.68	0.78
M17 SW	0.33	4.8	2.23	0.74
G012.02-00.03	0.60	1.2	1.59	0.62
W43	0.38	2.8	2.10	0.76
M16	0.29	3.3	2.15	0.81
Average	0.40 ± 0.09	2.94 ± 1.27	2.16 ± 0.30	0.74 ± 0.06

Columns: (1) GMC names (2) The fitting parameter of the non-linear relation. (3) The coefficient of the spectrum column density (SCD$_{\rm C}$). (4) The mean value of the $X_{\rm CO}$ factor in a GMC. (5) Correlation coefficient. The errors of averaged value are adopted as the standard variation in all GMCs.

where r_e = 6.2 kpc is the scale radius of Galactic disc and X_0 is $X_{\rm CO}$ at $R = R_0$ = 8.0 kpc (VERA Collaboration et al. 2020; Reid et al. 2019). This equation can be deformed as follows.

$$X_{\rm CO} = 0.59 \times 10^{20} \exp\left(\frac{R}{6.567\ [{\rm kpc}]}\right)\ [{\rm cm^{-2}(K\ km\ s^{-1})^{-1}}] \quad (12)$$

Figure 5 shows a plot of the $X_{\rm CO}$ factor obtained in this paper as a function of the Galactocentric distance. It is found that $X_{\rm CO}$ increases with the distance from the Galactic Centre, and the plot may be fitted by an exponential function by

$$X_{\rm CO} = 1.48 \times 10^{20} \exp\left(\frac{R}{14.07[{\rm kpc}]}\right)\ [{\rm cm^{-2}(K\ km\ s^{-1})^{-1}}]. \quad (13)$$

Our fitting result yields a significantly larger $X_{\rm CO}$ at the Galactic Centre by a factor of 3 compared to that by Arimoto et al. (1996) indicated by the green dotted line. This discrepancy may be caused by no data point within $R < 2$ kpc in our study as well as by the normalization of the local value to 2×10^{20} [H$_2$ cm^{-2}(K km s^{-1})$^{-1}$

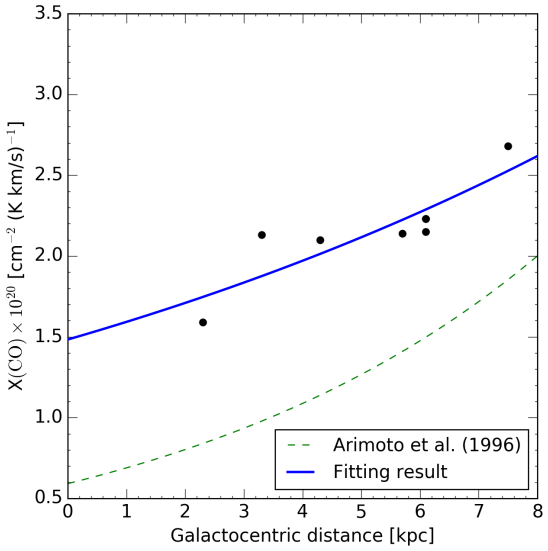

Figure 5. The $X_{\rm CO}$ gradient from the distance of the Galactic Center. The blue line shows the fitting result adopted by the exponential function.

The green dashed line indicates the relation from Arimoto et al. (1996).

at 8 kpc in the previous study. Sodroski et al. (1995) reported that the $X_{\rm CO}$ factor within 400 pc in the Galactic Centre region is by a factor 3-10 lower than the Galactic disk. Therefore, the value of $X_{\rm CO}$ in the Galactic Centre is still controversial. The present method applied to the ^{12}CO and ^{13}CO J =1-0 line data in the Galactic Centre region would provide with a more precise determination of $X_{\rm CO}$ in the innermost Milky Way. A detailed analysis of this point will be presented in a separate paper using the CO survey data of the Galactic Centre (e.g., Oka et al. 1998; Torii et al. 2010; Tokuyama et al. 2019).

6 SUMMARY

The conclusions of this paper are summarized as follows:

(i) We studied the correlation between ^{12}CO and ^{13}CO intensities toward the Galactic GMCs W51A, W33, N35-N36 complex, W49, M17SW, G12.02-00.03, W43, and M16 using the FUGIN CO survey data taken with the Nobeyama 45 m telescope.

(ii) All the GMCs show intensity saturation of the ^{12}CO line in regions with high brightness of ^{13}CO.

(iii) We also presented high-resolution $X_{\rm CO}$ factor maps made from the correlations of the CO isotopologues, which revealed local variability of the factor in each GMC. We also showed that the $X_{\rm CO}$ factor monotonically decreases with increasing ^{12}CO brightness temperature.

(iv) The averaged value of all GMCs is calculated to be $X_{\rm CO} = (2.16 \pm 0.30) \times 10^{20}$ cm^{-2} (K km s^{-1})$^{-1}$, which is consistent within the error with the reported values in the previous review.

(v) We showed that the $X_{\rm CO}$ increases with the Galactocentric distance in accordance with the previous works, while suggesting a smaller value in the GC by a factor of 3.

ACKNOWLEDGEMENTS

The Nobeyama 45-m radio telescope is operated by the Nobeyama Radio Observatory. We utilized the Python software package for astronomy (Astropy Collaboration et al. 2013), NumPy (van der Walt et al. 2011), Matplotlib (Hunter 2007), IPython (Perez, & Granger 2007), and APLpy (Robitaille & Bressert 2012).

Data availability The data underlying this article are available in http://nro-fugin.github.io. The FUGIN CO data were retrieved from the JVO portal http://jvo.nao.ac.jp/portal operated by ADC/NAOJ.

REFERENCES

Abdo, A. A., Ackermann, M., Ajello, M., et al. 2010, ApJ, 710, 133
Arimoto, N., Sofue, Y., & Tsujimoto, T. 1996, PASJ, 48, 275 8, 275
Astropy Collaboration, Robitaille, T. P., Tollerud, E. J., et al. 2013, A&A, 558, A33
Blitz, L., Fukui, Y., Kawamura, A., et al. 2007, Protostars and Planets V, 81. doi:10.48550/arXiv.astro-ph/0602600
Bloemen, J. B. G. M., Strong, A. W., Mayer-Hasselwander, H. A., et al. 1986, A&A, 154, 25
Bolatto, A. D., Wolfire, M., & Leroy, A. K. 2013, ARA&A, 51, 207
Chevance, M., Krumholz, M. R., McLeod, A. F., et al. 2022, arXiv:2203.09570. doi:10.48550/arXiv.2203.09570
Dame, T. M., Hartmann, D., & Thaddeus, P. 2001, ApJ, 547, 792. doi:10.1086/318388
Dickman, R. L. 1978, ApJS, 37, 407
Dobbs, C. L., Krumholz, M. R., Ballesteros-Paredes, J., et al. 2014, Protostars and Planets VI, 3. doi:10.2458/azu_uapress_9780816531240-ch001
Frerking, M. A., Langer, W. D., & Wilson, R. W. 1982, ApJ, 262, 590
Fukui, Y., Okamoto, R., Kaji, R., et al. 2014, ApJ, 796, 59. doi:10.1088/0004-637X/796/1/59
Fukui, Y. & Kawamura, A. 2010, ARA&A, 48, 547. doi:10.1146/annurev-astro-081309-130854
Fujita, S., Torii, K., Kuno, N., et al. 2021, PASJ, 73, S172. doi:10.1093/pasj/psz028
Fujita, S., Ito, A. M., Miyamoto, Y., et al. 2023, PASJ, 75, 279. doi:10.1093/pasj/psac104
Hayashi, K., Okamoto, R., Yamamoto, H., et al. 2019, ApJ, 878, 131
Hayashi, K., Mizuno, T., Fukui, Y., et al. 2019, ApJ, 884, 130
Heyer, M. & Dame, T. M. 2015, ARA&A, 53, 583. doi:10.1146/annurev-astro-082214-122324
Hunter, J. D.¥ 2007, Computing in Science and Engineering, 9, 90
Kamazaki, T., Okumura, S. K., Chikada, Y., et al. 2012, PASJ, 64, 29. doi:10.1093/pasj/64.2.29
Kohno, M., Torii, K., Tachihara, K., et al. 2018, PASJ, 70, S50. doi:10.1093/pasj/psx137
Kohno, M., Tachihara, K., Torii, K., et al. 2021, PASJ, 73, S129. doi:10.1093/pasj/psaa015
Kuno, N., et al. 2011, in Proc. 2011 XXXth URSI General Assembly and Scientific Symposium (New York: IEEE), 3670 [1]
Lee, M.-Y., Stanimirović, S., Wolfire, M. G., et al. 2014, ApJ, 784, 80. doi:10.1088/0004-637X/784/1/80
Lee, C., Leroy, A. K., Bolatto, A. D., et al. 2018, MNRAS, 474, 4672. doi:10.1093/mnras/stx2760
Leroy, A. K., Bolatto, A., Gordon, K., et al. 2011, ApJ, 737, 12
Lin, S.-J., Shimajiri, Y., Hara, C., et al. 2016, ApJ, 826, 193. doi:10.3847/0004-637X/826/2/193
Liszt, H. S., Pety, J., & Lucas, R. 2010, A&A, 518, A45. doi:10.1051/0004-6361/201014510

[1] http://ieeexplore.ieee.org/xpl/articleDetails.jsp?arnumber=6051296

Lombardi, M., Alves, J., & Lada, C. J. 2006, A&A, 454, 781. doi:10.1051/0004-6361:20042474
Minamidani, T., Nishimura, A., Miyamoto, Y., et al. 2016, Proc. SPIE, 99141Z
Miyawaki, R., Hayashi, M., & Hasegawa, T. 2022, PASJ, 74, 128. doi:10.1093/pasj/psab113
Mizuno, N., Rubio, M., Mizuno, A., et al. 2001, PASJ, 53, L45. doi:10.1093/pasj/53.6.L45
Muraoka, K., Homma, A., Onishi, T., et al. 2017, ApJ, 844, 98. doi:10.3847/1538-4357/aa7a0b
Nakajima, T., Inoue, H., Fujii, Y., et al. 2019, PASJ, 71, S17. doi:10.1093/pasj/psy112
Nishimura, A., Minamidani, T., Umemoto, T., et al. 2018, PASJ, 70, S42. doi:10.1093/pasj/psx149
Nishimura, A., Fujita, S., Kohno, M., et al. 2021, PASJ, 73, S285. doi:10.1093/pasj/psaa083
Ohno, T., Tokuda, K., Konishi, A., et al. 2023, arXiv:2304.00976. doi:10.48550/arXiv.2304.00976
Oka, T., Hasegawa, T., Sato, F., et al. 1998, ApJS, 118, 455. doi:10.1086/313138
Okamoto, R., Yamamoto, H., Tachihara, K., et al. 2017, ApJ, 838, 132
Perez, F., & Granger, B. E. 2007, Computing in Science and Engineering, 9, 21
Pitts, R. L. & Barnes, P. J. 2021, ApJS, 256, 3. doi:10.3847/1538-4365/ac063d
Planck Collaboration, Ade, P. A. R., Aghanim, N., et al. 2011, A&A, 536, A19. doi:10.1051/0004-6361/201116479
Planck Collaboration, Fermi Collaboration, Ade, P. A. R., et al. 2015, A&A, 582, A31
Pineda, J. E., Caselli, P., & Goodman, A. A. 2008, ApJ, 679, 481
Remy, Q., Grenier, I. A., Marshall, D. J., et al. 2017, A&A, 601, A78
Reid, M. J., Menten, K. M., Brunthaler, A., et al. 2019, ApJ, 885, 131. doi:10.3847/1538-4357/ab4a11
Robitaille, T., & Bressert, E. 2012, APLpy: Astronomical Plotting Library in Python, ascl:1208.017
Rosolowsky, E., Engargiola, G., Plambeck, R., et al. 2003, ApJ, 599, 258. doi:10.1086/379166
Sakamoto, S. 1996, ApJ, 462, 215. doi:10.1086/177142
Sanna, A., Reid, M. J., Menten, K. M., et al. 2014, ApJ, 781, 108. doi:10.1088/0004-637X/781/2/108
Sawada, T., Ikeda, N., Sunada, K., et al. 2008, PASJ, 60, 445. doi:10.1093/pasj/60.3.445
Scoville, N. Z., Yun, M. S., Clemens, D. P., et al. 1987, ApJS, 63, 821. doi:10.1086/191185
Sodroski, T. J., Odegard, N., Dwek, E., et al. 1995, ApJ, 452, 262. doi:10.1086/176297
Sofue, Y., & Kataoka, J. 2016, PASJ, 68, L8
Sofue, Y., Kohno, M., Torii, K., et al. 2019, PASJ, 71, S1
Sofue, Y. 2019, PASJ, 71, 104. doi:10.1093/pasj/psz090
Sofue, Y. 2019, PASJ, 71, 121. doi:10.1093/pasj/psz106
Sofue, Y. 2020, PASJ, 72, 21. doi:10.1093/pasj/psz143
Sofue, Y. 2020, MNRAS, 492, 5966
Sofue, Y. & Kohno, M. 2020, MNRAS, 497, 1851. doi:10.1093/mnras/staa2056 (Paper I)
Sofue, Y. 2021, Galaxies, 9, 13. doi:10.3390/galaxies9010013
Sofue, Y. 2022, MNRAS, 509, 5809. doi:10.1093/mnras/stab3091
Solomon, P. M., Rivolo, A. R., Barrett, J., et al. 1987, ApJ, 319, 730
Strong, A. W., Bloemen, J. B. G. M., Dame, T. M., et al. 1988, A&A, 207, 1
Tokuyama, S., Oka, T., Takekawa, S., et al. 2019, PASJ, 71, S19. doi:10.1093/pasj/psy150
Torii, K., Kudo, N., Fujishita, M., et al. 2010, PASJ, 62, 1307. doi:10.1093/pasj/62.5.1307
Torii, K., Fujita, S., Matsuo, M., et al. 2018, PASJ, 70, S51. doi:10.1093/pasj/psy019
Torii, K., Fujita, S., Nishimura, A., et al. 2019, PASJ, 71, S2. doi:10.1093/pasj/psz033
Umemoto, T., Minamidani, T., Kuno, N., et al. 2017, PASJ, 69, 78
van der Walt, S., Colbert, S. C., & Varoquaux, G. 2011, Computing in Science and Engineering, 13, 22
VERA Collaboration, Hirota, T., Nagayama, T., et al. 2020, PASJ, 72, 50. doi:10.1093/pasj/psaa018
Wilson, C. D. 1995, ApJ, 448, L97. doi:10.1086/309615
Yamagishi, M., Kaneda, H., Ishihara, D., et al. 2016, ApJ, 833, 163. doi:10.3847/1538-4357/833/2/163
Yoda, T., Handa, T., Kohno, K., et al. 2010, PASJ, 62, 1277. doi:10.1093/pasj/62.5.1277